# Global and local structural behavior of lattice steel transmission towers with semi-rigid connections

Feleki Attila
Civil Engineering and Building Services
Technical University of Cluj-Napoca
Cluj-Napoca, Romania
attila.feleki@cif.utcluj.ro

Nagy Zsolt
Civil Engineering and Building Services
Technical University of Cluj-Napoca
Cluj-Napoca, Romania
zsolt.nagy@dst.utcluj.ro

*Abstract*: *The paper deals with failure mechanism methodology analysis of lattice steel transmission towers (LSTT). The methodology combines the following: elastic and buckling 3D analysis using Consteel software, connection design resistance and stiffness analysis using IDEA StatiCa, on-site evaluation about general condition of LSTTs combined with 3D laser scanning, respectively nonlinear pushover and time-history analyses using SAP2000.*

*Keywords—lattice steel transmission tower; structural analysis; buckling sensitivity; joint semi-rigidity; wind loads; laser scanning; point cloud; nonlinear analyses; collapse mechanisms.*

## I. INTRODUCTION

The profession of design engineer requires not only a position with significant responsibility, but also requires an attitude of dedication and professionalism. For this reason, the design and verification of all types of structures, regardless of their complexity, must be developed with adequate competence. Challenges must be met with professional curiosity, and instead of simplistic approximations, calculations and analyzes must be complemented by in-depth research.

Analyzing the information available in freehand technical drawings that are often over 50 years old (Fig. 1), a series of questions were raised in the author's mind. Going through the regulations and structural requirements in force, these questions have multiplied instead of being answered. Regarding the experiences during the 3D structural analyzes, the questions multiplied again. In order to solve it, the authors formulated a series of questions in the field of structural analysis of LSTTs: a) How to properly model the design loads, respectively the structure of the columns in a 3D calculation software? b) What type of joints are used between the tower elements? What is the stiffness class of these joints? c) In which manner can be quantified the general condition of LSTTs on field? d) What is the effect of the joints in the maximum elastic and plastic capacities for LSTTs? e) What are the critical elements responsible for the failure, and what is the collapse procedure?

The possibility of full-scale tower tests is vastly limited because of financial and time-consuming aspects [1]. However, there is another straightforward solution, which is the investigation of on-site degraded or collapsed towers structures.



Fig. 1. LSTT network service live status in Romania
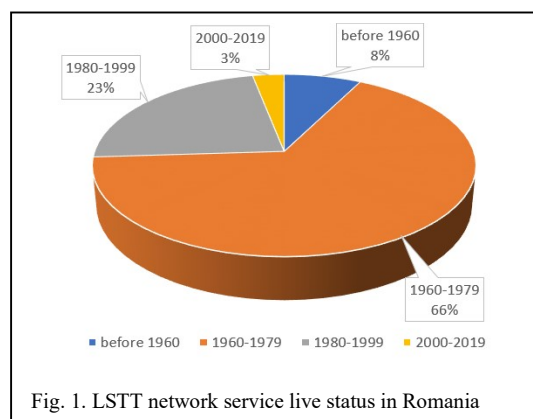
The aim of this research is to develop a multidisciplinary methodology which gives an objective standpoint to engineers in the practical design field.

## II. JOINT ANALYSIS AND CLASSIFICATION

It is noted that the effect of joints has a particularly important role in the behavior of metal structures. The regular calculation methods performed in the daily design procedures do not consider the complex behavior of the bolted joints of the LSTTs. This behavior can be explained by eccentric and overlapping joints, which lead to the defense of a parasitic effect in the overall analysis.

### A. Details of analytically studiet joints

Bolted connections of LTTs are the main load-transferring structural components. Since the global configuration of towers consists of recurrent details and solutions, the joints can also be classified into 3 categories: (I) spliced and lapped connections between primary members (e.g. leg members), (II) bolted gusset plate connections of diagonals, and (III) welded and bolted connections of secondary elements.

To determine the basic properties of strength, rigidity and stability, a general analysis has been carried out using Idea StatiCa software [2]. The 3D joint calculation models were built based on the available details from original production and assembly plans drawn in 1960's (Fig. 2). The software operates on a so-called component-based finite element method
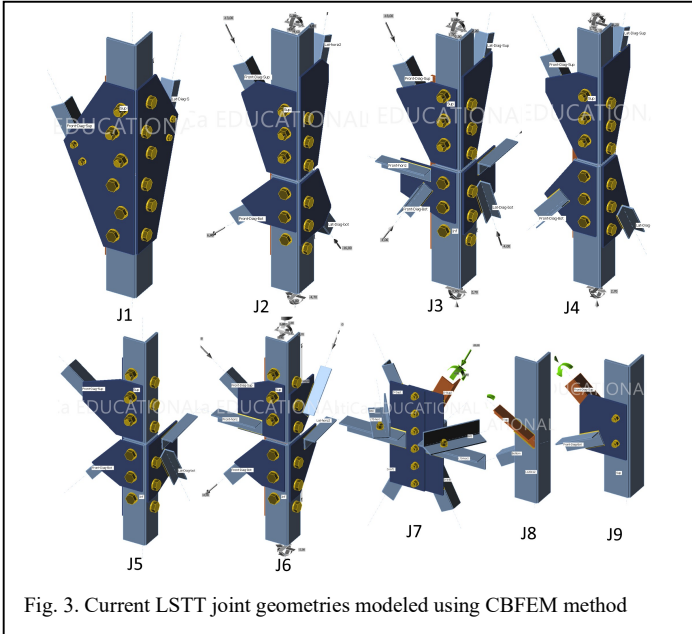
Fig. 3. Current LSTT joint geometries modeled using CBFEM method

(CBFEM), which uses geometrically and materially nonlinear analysis (GMNA). The angle profiles eccentricities have been taken into consideration in the calculation process, and in regards to the material, S235 steel was used for profiles and plates, respectively class 5.6. quality for bolts.

As a partial result of the calculations, each connection complied with the structural requirements under loadings based on current regulations. However, the objective of the analyzis was to determine the maximum capacity and the rigidity of studied joints.

The consesus has been the traditional approach of pin/hinge type for all joints in the global analysis (even for the lapped leg connections, which normally contain up to 10-14 bolts). Using this method, the calculation complexity is reduced, but previous research showed that this simplification presents considerable discrepancies in results compared to complex numerical models or experiments. In orded to refute the pinned truss theory, a bending moment capacity evaluation was performed for the spliced lapped leg connections. Additionally, a comprehensive stiffness analysis has been carried out, classifying the joints as nominally pinned, semi-rigid or rigid, according to their initial rotational stiffnesses $S_{j,ini}$. It can be observed that the splice lapped connections present a significant bending moment capacity, and also, that 8 out of the 9 analysed joints present a semi-rigid behaviour. To validate the CBFEM analysis, joint failure modes were compared to on-site collapsed towers connections.

TABLE 1

| Joint | Angle profile | Bending moment capacity | |
|---|---|---|---|
| | | $M_y$ [kNm] | $M_z$ [kNm] |
| J1 | L140x12, L70x6, L60x6 | 18.60 | 21.60 |
| J2 | L140x12, L70x6, L60x6 | 20.70 | 20.70 |
| J3 | L140x12, L120x12, L70x6, L60x6 | 15.75 | 15.60 |
| J4 | L140x12, L120x12, L70x6, L60x6 | 15.67 | 15.67 |
| J5 | L120x12, L70x6, L60x6 | 15.15 | 13.56 |
| J6 | L120x12, L120x10, L70x6, L60x6 | 13.38 | 13.38 |

TABLE 2

| Joint | $S_{j,ini}$ [kNm/rad] | | Rigidity class | | Class limits [kNm/rad] | |
|---|---|---|---|---|---|---|
| | $M_y$ | $M_z$ | $M_y$ | $M_z$ | Rigid | Pinned |
| J1 | 1757 | 751 | semi-rigid | | 5948 | 37 |
| J2 | 6238 | 1291 | semi-rigid | | 8699 | 543 |
| J3 | 2333 | 1130 | semi-rigid | | 4719 | 295 |
| J4 | 1881 | 788 | semi-rigid | | 6182 | 386 |
| J5 | 855 | 340 | semi-rigid | pinned | 6182 | 386 |
| J6 | 4550 | 1103 | semi-rigid | | 5259 | 329 |
| J7 | 1335 | 40 | rigid | pinned | 318 | 20 |
| J8 | 183 | 77 | semi-rigid | | 383 | 24 |
| J9 | 310 | 22 | semi-rigid | pinned | 383 | 24 |

As observed in Fig. 3, the tension and plastic strain maps are in good correlation with the on-site deformed shapes.

Similarly to Mills` results [3], the splice lapped connections showed net section (tearing) failure in the local region with significant bolt hole elongations, respectively in the other case, overall buckling failure can be observed near the transition between the beam and plate elements.
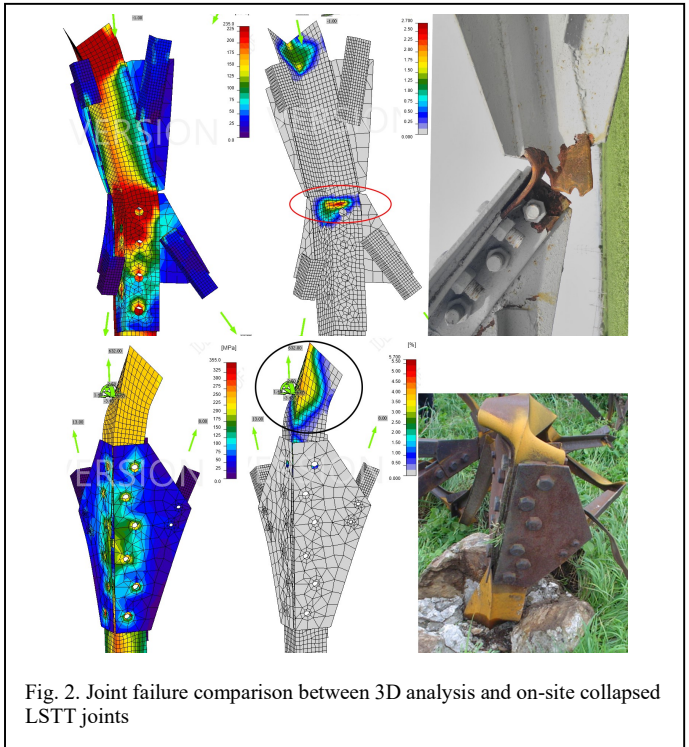


Fig. 2. Joint failure comparison between 3D analysis and on-site collapsed LSTT joints

III.  MODELING OF LSTTs

A.  General information about LSTTs

An overhead transmission line connects two nodes of the power supply grid. Depending on their position in the line, various types of towers can be distinguished such as: suspension towers (ST), angle suspension towers (AST), angle tension towers (AT), tension towers (TT) and, terminal towers (TT). Tension towers serve as rigid points, able to prevent progressive collapse of the entire line.

Much attention has been drawn to the evaluation of meteorological loadings of LSTTs. Depending on different national requirements, the theoretically identical actions are considered under completely different conditions, which leads to considerably different loading values. To highlight these deviations, the resultant concentrated wind load acting on the structure of an angle tension tower was calculated and compared in accordance with 6 different standards (Fig. 2): 1L-1-67 (Romanian code from 1967), NTE 0030400 (actual Romanian code), MSZ 151-1 (Hungarian code used between 2000-2013, since that it was switched to EN), ASCE 07-10 (American code), EN 50341 (Eurocode) and IS 802-1-1:2015 (Indian code). In the comparison process, the effect of ice is not considered, as the requirements related to wind loads simultaneously with ice deposition are treated separately in national standards.
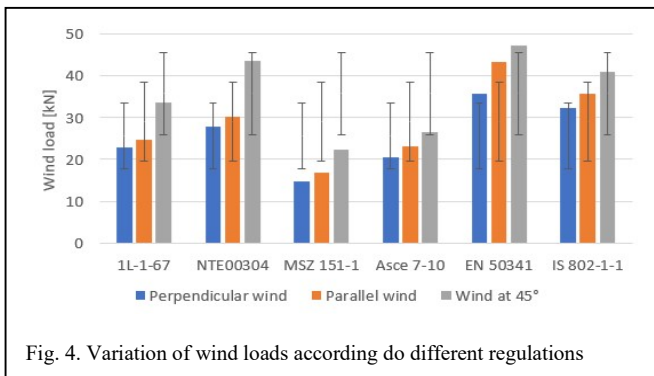


Fig. 4. Variation of wind loads according do different regulations

The data in Fig. 2. emphasize that the difference between the old and actual Romanian code is not substantial. However, wind evaluation according to new EN and IS codes gives considerably higher values.

To cover all the loads acting on the structures, the following unit loads were taken into account in the calculation and design check of LSTT elements:

- dead loads including the weight of the total structure and its attachments (conductors and equipment).
- ice, rime or wet snow on the tower itself, respectively on conductors and equipment.
- wind pressure on tower structure and conductors, covered and not covered with ice.
- loads from conductor tensile forces acting on cross-arms.

## B. Structural modeling of LSTTs

Modeling of these type of structures, even at initial phase, with theoretically perfect conditions, presents a significant challenge to design engineers due to their complex geometry and structural configuration [3]. For the best possible results, several modeling aspects were analyzed:

- influence of rotation angle of the members – in the case of incorrect leg member rotation, a 5 % difference may occur in the structural utilization percentage.

- definition of geometrical eccentricity – when taking into consideration the eccentricity of the angle profiles in global analysis, parasitic second-order effects may influence the analysis, thereby providing unreliable results.
- cross-arm and tower apex configuration – there is a considerable difference between the calculation model and executed structure, since in the theoretical version the members axes intersect in one point, and in the case of real tower these elements are connected with plates, thereby forming a significantly less stable square configuration. If this aspect is modeled, the cross-arm and apex angle profiles will sustain a torsional bending moment, causing a substantial jump in structural utilization percentages.

## C. Case study – Angle tension tower

A standard angle tension tower was chosen for further detailed analyses. This configuration is commonly used in Romania since 1976 by the Romanian Energy Regulatory Authority. The tower was designed for alignment angles of $\alpha=200^g\div140^g$, has a 28,7 m height with a 5,00 x 3,50 base size. Detailed configuration, dimensions and member cross sections are shown in Fig. 5.

The model was analyzed with commercial software Consteel V14, which uses warping as $7^{th}$ degree of freedom. To identify the most sensitive elements in terms of stability loss, buckling sensitivity analysis was performed. In this procedure, all members are assigned with the most relevant buckling mode in each load combination. To quantify this phenomenon, the general method from EN 1993-1-1 6.4. was used, which calculates the structural utilization percentage with the help of the minimum load amplification factor $\alpha_{cr}$.
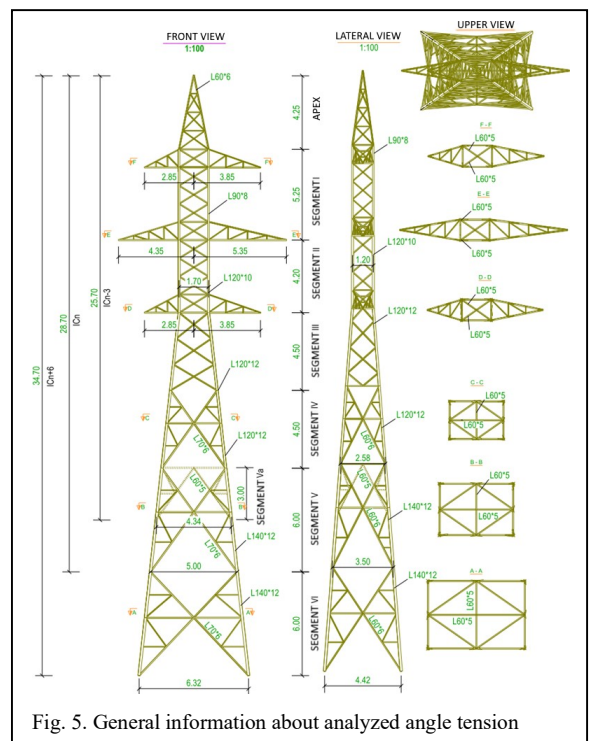


Fig. 5. General information about analyzed angle tension

In order to take into consideration the most unfavorable meteorological condition, linear static analysis was employed for a number of load combinations both at normal and at damaged operating mode: N1 (maximum wind perpendicular to the line), N2 (wind perpendicular to the line, simultaneously with ice deposition), N3 (maximum wind parallel to the line), N4 (wind along the line, simultaneously with ice deposition), D1 (conductor breaking in condition of a wind perpendicular to the line, simultaneously with ice deposition). Out of these combinations, N2 and D1 were the most unfavorable ones. Despite the fact that conductor breaking produces a significant global torsion effect in the tower, the critical axial efforts are found in combination N2.

To solve the vital problem of the influence of joint rigidity on global structural capacity, an extensive comparative study with 4 different configurations has been made:

- pinned model: all bars are pinned.
- semi-rigid model: all joints are semi-rigid, except the connections with one bolt.
- model with pinned diagonals and rigid leg members.
- model with rigid members: all bars have continuous ends.

The results of the study are presented in Table 3, with maximum structural utilizations, and associated locations.

TABLE 3

| Model description | Pinned joints | Semi-rigid joints | Pinned diagonals, rigid leg | Rigid joints |
|---|---|---|---|---|
| Max. structural utilization [%] Combination N2 | 95,8 | 110,4 | 138,2 | 137,3 |
| Location | Leg member S4 | Joint between S5-S4 | Joint between S5-S4 | Joint between S5-S4 |

It is shown that there is a substantial difference between the utilization percentages (up to 43 %), the semi-rigid model being positioned in the middle of the field. For a more detailed overview, the buckling resistance of each primary structural element has been calculated using the eigenvalue and effective length factor.

IV.     3D LASER SCANNING OF A LSTT

The 3D laser scanning process, otherwise called terrestrial photogrammetric technology, analyzes an object or the environment to collect information about its form and shape. Furthermore, it can record different aspects such as color. The collected data can be used to build three-dimensional digital models that are compatible with different high-performance processing programs. Laser scanning has been developed in the second half of the 20th century, aiming to recreate different surfaces with high precision. The methodology is specifically used in the field of academic research, respectively industrial, architectural and civil surveying [4].

In civil engineering, laser scanning consists of the controlled process of laser-beam steering and distance measurement at each scanned point. This allows identification of the 3D position of each point in the scanned image.
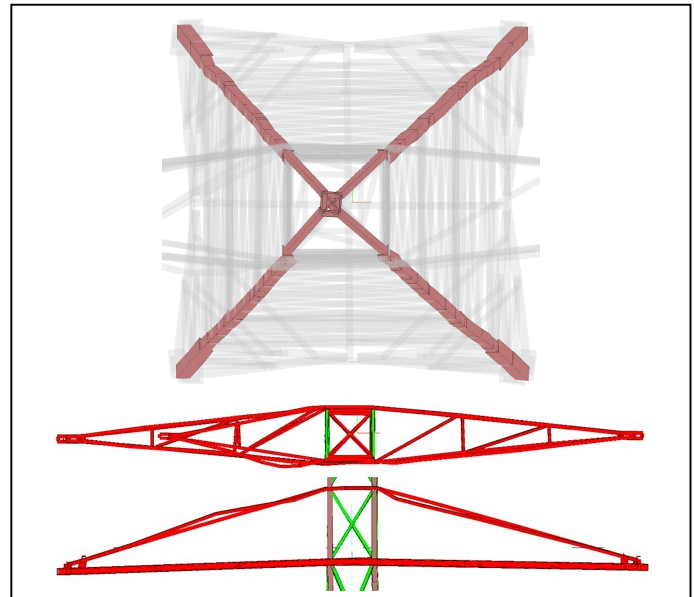


Fig. 6. Deformed leg member and cross-arm geometries processed from 3D point cloud

In general, a single scan will not produce a sufficiently detailed pattern, so it is necessary to perform multiple measurement stations in different directions. These scans must be imported into a common reference system, to align and overlap the recordings. After removing unnecessary details and filtering the points that are not part of the scanned object (such as trees or cables), the point cloud can be processed.

The greatest advantage of the process is that laser scanning is non-destructive and does not endanger people's lives. Taking advantage of this, 3D scanning is most often used in the analysis of bridges and heritage buildings. Yet, the state of the art of national and international literature shows that this technology has not been widely used in the study of LSTTs.

The laser scanning was performed on a suspension tower, using a Trimble TX8 device which has the following main specifications: maximum range of 340 m, scan speed of 1 million dots/sec and 10 MP resolution integrated HDR camera.

It is worth mentioning that the exposure of the tower is a significant factor, since the scanning device requires a flat, obstacle-free area for its operation. The height of the scanned tower was 32,2 m, with base dimensions of 2,41 m × 2,41 m. The scan was performed from 8 different locations, which led to a united point cloud with 22.44 million points. Due to the complex quality of the scanning, the point cloud processing could be performed efficiently after overlapping the point cloud with the initially built undeformed 3D model. This operation was realized in Tekla Structures BIM software.

As the result of the laser scanning process, an axonometry was created which corresponds to the actual on-site geometry. With the help of this 3D model, geometrical deviations can be measured, which helps in the classification of the structure (Table 4 and 5). Also, it can be used for detailed structural analyses to determine the capacity of the tower.

TABLE 4

| Criteria | Height / Length [m] | Limit value | | Measured value | |
|---|---|---|---|---|---|
| | | [mm] | | | |
| Tower verticality | 32,3 | 63,8 | H/500 | 174 | |
| Inferior cross-arm horizontality | 4,1 | 20,5 | L/200 | 80 | 147 |
| Superior cross-arm horizontality | 2,6 | 13 | | 69 | |

TABLE 5

| Tower | Deformations | | | | Joints | | Corrosion | |
|---|---|---|---|---|---|---|---|---|
| | Global | | Local | | | | | |
| | Main legs | Cross-arms | Main bracing | 2nd bracing | Plate | Bolt | Angle | Plate |
| TT | 8/10 | 7/10 | 7/10 | 6/10 | 8/10 | 9/10 | 4/10 | 6/10 |

After the reevaluation of loads, where the specific on-site alignment of the structure was accounted, a design (N1) and a serviceability load combination (S1) were created, where the value of maximum wind perpendicular to the line was investigated. Since the laser scanning was realized in the summer, these values did not take into consideration the ice loading on the conductors. Fig. 8. a) presents the first buckling shape with eigenvalue of 1,81 for design combination N1, respectively 2,29 for serviceability combination S1. The structural utilization for N1 is 129,9 %, while for S1 is 102 %. In both cases, the critical element is the compressed L70x7 leg member, near the segment connection. This location is in good correlation with the experienced on-site collapse modes.



a) first buckling mode  b) combination N1  c) combination S1
Fig. 7. Results of laser scanned tower for design and serviceability loads
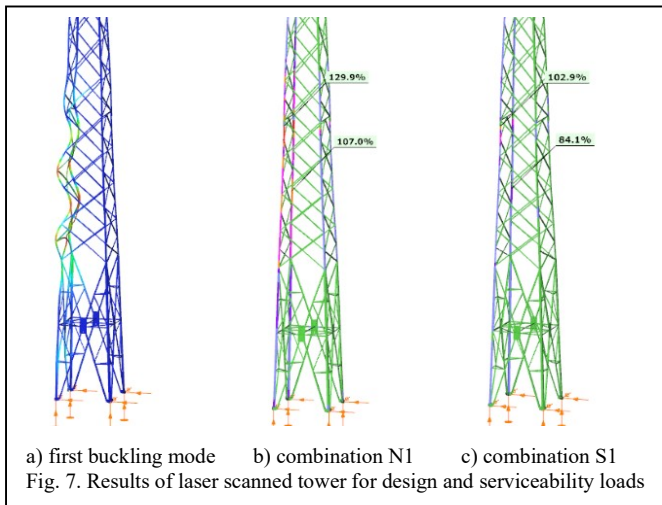
It can thus be suggested that the tower would fail in the case of a greater wind load than specified in the code (30 daN/m² - 22,13 m/s - 79,6 km/h), or in the presence of simultaneous ice and wind loading - which is clearly the more critical phenomenon. These observations have strong implications as the main required information from client's side in the case of an expertizing project.

To sum up, the tower barely meets the structural requirements for the serviceability load case, from which follows that the tower would fail under the maximum wind and ice load case. This demonstrates the general criticality of the condition of LSTT structures.

## V. ON-SITE EVALUATION OF STRUCTURAL CONDITION

The principle of this method is to classify the different structural properties in a clear manner with grades from 1÷10, based on the requirements of the normative [5] *Methodology for the design of rehabilitation works of 110 kV OHL.*

Using this method, the expertizing engineer can effectively highlight the objective status of any investigated tower. The table is filled after on-site survey.

## VI. NON-LINEAR PUSHOVER AND TIME-HISTORY ANALYSIS

The non-linear analyses were carried out using commercial software SAP 2000 V20.1. For bar modeling beam/column elements were used, while for material properties a more complex method was adopted: non-deformed bars were collected from collapsed towers, on which tensile tests were performed, and these results were accounted. The theory of large displacements was also used. As reported previously, every main structural members buckling resistance has been determined, as well as the joints ultimate resistances. These capacities were substituted as axial plastic hinge limits, following FEMA 365 requirements. In an attempt to model the real behavior of LSTTs, the semi-rigidity of joints was also considered in the analysis, by comparing the previously described 4 rigidity models.

### A. Pushover analysis on angle tension tower

The pushover analysis was carried out on the angle tension tower presented on Fig. 5. The results of elastic analyses are also included in the pushover curves (Figure 8) to validate the analysis (Table 5). In addition, two main parameters have been introduced to highlight the inelastic characteristics [6]: ductility capacity (CAD) and over-resistance (ORS).

Figure 8 and Table 6 demonstrates the substantial influence of connection rigidity in ultimate capacity. The most conservative approach is the pinned theory, while the semi-rigid model presents a 13,4 % bigger capacity, while being in the middle field compared to all models. The residual resistance of semi-rigid or rigid models can be the explanation why these structures survived extreme loading conditions, suffering only local damages [7]- [8].
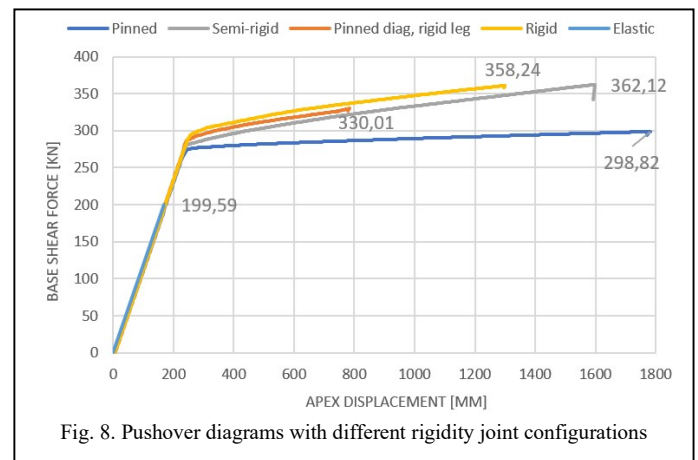


Fig. 8. Pushover diagrams with different rigidity joint configurations

TABLE 6

| Inelastic data | Pinned model | | Semi-rigid model | | Pinned diagonals, rigid leg | | Rigid model | |
|---|---|---|---|---|---|---|---|---|
| | $V_{base}$ [kN] | Drift [%] | $V_{base}$ [kN] | Drift [%] | $V_{base}$ [kN] | Drift [%] | $V_{base}$ [kN] | Drift [%] |
| Failure | 320 | 4,68 | 363 | 5,52 | 351 | 4,15 | 365 | 5,22 |
| Critical bar | Leg of S6 | | Leg of S6 | | Leg of S6 | | Lateral diagonal of S6 | |
| CAD | 5,78 | | 6,48 | | 4,89 | | 6,06 | |
| ORS | 1,59 | | 1,80 | | 1,70 | | 1,81 | |

## B. Time history analysis on a suspension tower

Understanding complex structures collapse mechanism is quite a challenge for structural engineers, but being able to going through this process, helps the overall knowledge of the design. The authors developed a method which makes this possible, and validated it on a widely used suspension tower. The procedure consists of the following steps (Figure 9):

a) static linear analysis to determine the efforts and deformations in the tower (17,09 kN base shear force, 298 mm horizontal deformation at apex).

b) static linear elastic buckling sensitivity analysis to calculate the buckling resistance of primary structural members.

c) joint analysis for the classification of rotational stiffnesses and ultimate capacities ($S_{js,My}$=700 kNm/rad, $S_{js,Mz}$=400 kNm/rad).

d) nonlinear static Pushover analysis in order to specify the critical element, and the inelastic properties (middle segment compressed L70x7 leg member, CAD=4,24, ORS=2,85),

e) nonlinear dynamic Time history analysis, where the critical element is instantaneously removed, and the analysis is performed until the structure collapses (drift=4,86%, base shear=48,72 kN).

As illustrated in Figure 9, the resulted collapse geometry is in good correlation with the on-site failed towers geometry.

## VII. CONCLUSIONS

The best practice is a good theory. Yet, as highlighted in this paper, the theory behind the design of LSTTs is full of uncertainties, and numerous requirements can be interpreted in different ways. This study clarifies these uncertainties.

The paper summarizes general structural design aspects of LSTTs, such as joint failure and rigidity, wind load magnitude differences in function of different codes, and influence of different modeling aspects. A laser scanning procedure is presented, where the real geometry of the tower is analyzed, and the ultimate wind load is investigated. The influence of joint semi-rigidity on static linear and nonlinear pushover analyses are reviewed, presenting the ultimate capacity and the critical failure member of the analyzed LSTT. Nonlinear dynamic time-history is used to determine the collapse mechanism, and the method is validated with the help of on-site collapsed towers.

## REFERENCES

[1] L. Tian, L. Guo, R. Ma, X. Gai, and W. Wang, "Full-scale tests and numerical simulations of failure mechanism of power transmission towers," Int. J. Struct. Stab. Dyn., vol. 18, no. 9, 2018

[2] A. Feleki and Z. Nagy, "Studies of behavior of lattice steel tower connections subjected to corrosion Modelling of steel lattice transmission towers Conclusions References," C65 Int. Conf. "Tradition Innov. 65 Years Constr. Transilv., pp. 4–5, 2019

[3] Lu C, Ou Y, Xinh Ma, Mills. JE, "Structural Analysis of Lattice Steel Transmission Towers: A Review," J. Steel Struct. Constr., vol. 2, no. 1, pp. 1–11, 2016

[4] I M. Ebrahim, "3D Laser Scanners: History, Applications and Future," L. LAMBERT Acad. Publ., no. October, p. 104, 2016

[5] Methodology for the design of rehabilitation works of 110 kV LSTT, ISPE-BUC, 1995

[6] T. H. Edgar and E. Sordo, "Structural behaviour of lattice transmission towers subjected to wind load," Struct. Infrastruct. Eng., vol. 13, no. 11, pp. 1462–1475, 2017

[7] P. S. Lee and G. McClure, "Elastoplastic large deformation analysis of a lattice steel tower structure and comparison with full-scale tests," J. Constr. Steel Res., vol. 63, no. 5, pp. 709–717, 2007

[8] B. Eltaly, A. Saka, and K. Kandil, "FE simulation of transmission tower," Adv. Civ. Eng., vol. 2014, 20
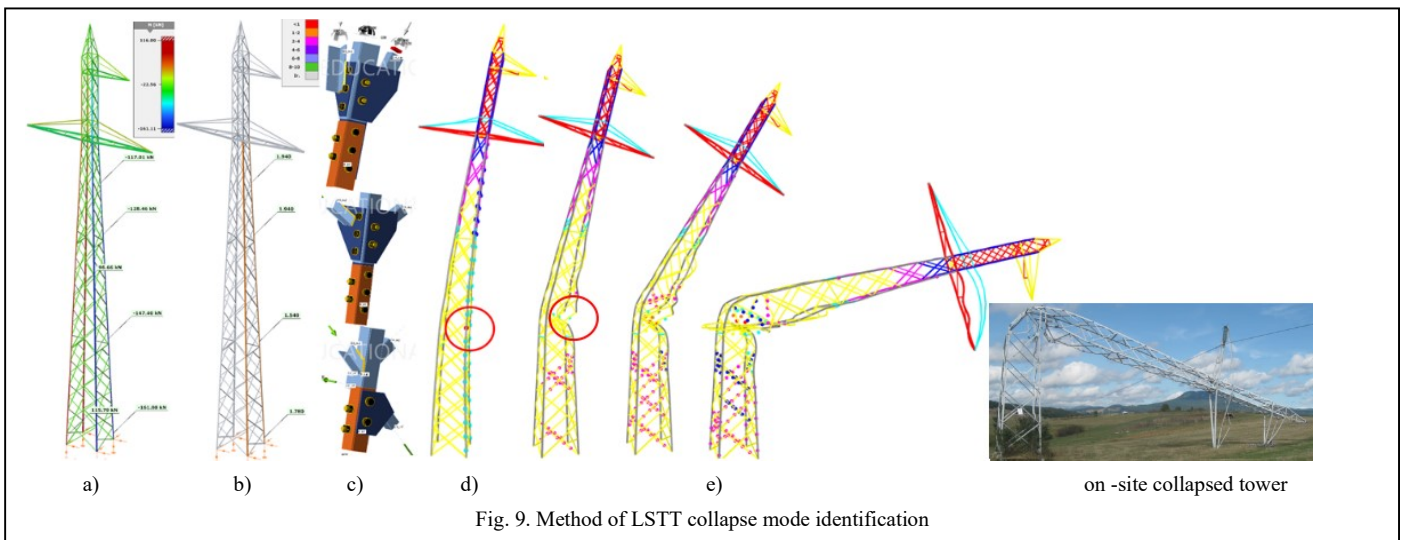
a)  b)  c)  d)  e)  on -site collapsed tower

Fig. 9. Method of LSTT collapse mode identification

# Behavior of embankment supported by rigid inclusions under static loads-parametric study

Rashad Alsirawan
*Széchenyi István University
Department of Structural and Geotechnical Engineering
H-9026 Győr, Hungary
E-mail: rashad.seirawan@gmail.com

Edina Koch
Széchenyi István University
Department of Structural and Geotechnical Engineering
H-9026 Győr, Hungary
E-mail: koche@sze.hu

*Abstract*— **Rigid inclusions has been gained popularity to support embankments over soft soil layers. The goal of rigid inclusions is to decrease the settlement and to improve the bearing capacity. The system contains the rigid elements, the load transfer platform and the reinforcement. Complex soil-structure interaction is developed due to the effect of the soil arching and tensioned membrane. In this paper, a validated 3D model of an embankment supported by rigid inclusions and two layers of geogrid are introduced based on a full-scale model with field measurements. The results highlight the effect of number and position of the geogrid layers on the load efficiency, add to that, the increase of the cover ratio by enlarging the column cap increases the load efficiency while the increase by enlarging the column cross-section area decreases the load efficiency.**

*Keywords— rigid inclusions; load efficiency; cover ratio.*

## I. INTRODUCTION

The demand of transportation grows in the last years, especially the high-speed railway lines. Sometimes, these lines need to be supported to fulfil the requirements of settlement and bearing capacity, essentially for the soft and weak soils. Sometimes, the piles can be overdesigned and the shallow foundations are not acceptable. In this case, the rigid inclusions technology is considered as a compromise solution [1].

The embankments over soft soils generally need to be supported by various technologies (rigid inclusions, stone columns, basal reinforcement with geosynthetics, prefabricated vertical drains) [2]. These technologies are used to enhance the shear resistance or to reduce the consolidation time of soft soils. Although the rigid inclusions outperform the other technologies to meet the aforementioned requirements, but this system is complex regarding the soil-structure interactions. The effects of soil arching, tensioned membrane and frictional interactions between the soil and geosynthetics represent the load transfer mechanism in this system. Due to the complexity and various interactions between the rigid inclusions' components, different researchers worked to clarify the behavior of rigid inclusions. a series of small-scale model tests performed by van Eekelen et al. [3] showed that the increase the internal friction angle improves the soil arching and using two layers of geogrid, on behalf of one, increases the load efficiency (defined as a ratio of vertical forces applied on the pile (column) to the total vertical forces in a unit cell) by a small amount. Girout et al. [4] performed thirty-three geotechnical centrifuge tests, and the findings were, increase

the embankment height increases the load efficiency, using geogrid layers improves the load efficiency, and the position and stiffness of the geosynthetic plays a main role of the load efficiency. Jenck [5] found, based on a small-scale model, that the increase of cover ratio increases the load efficiency. Blanc et al. [6] conducted a series of centrifuge tests, these tests showed that when the load transfer platform is thicker, the load efficiency is larger. Xu et al. [7] performed a series of scaled model tests, they concluded that the use of a cohesive soil as an embankment fill enhances the soil arching and hence the load efficiency. Okyay and Dias [8] conducted numerous model tests using centrifuges and concluded that the cover ratio is an important factor affecting the load efficiency.

Han and Gabr [9] used Flac program to perform a numerical analysis for the purpose of investigating the interactions between piles, soils, and geosynthetic layers. The researchers found that the load efficiency increases when the height of the embankment and the elastic modulus of the pile increases. Le Hello et al. [10] observed that the geosynthetic layers contribute in increasing the load efficiency as the pile network, the embankment height, and the cover ratio do. Wijerathna et al. [11] performed a 3D numerical model of rigid inclusion-supported embankment, Wijerathna et al. found that the load efficiency is affected by a small amount by the geosynthetic stiffness and column material stiffness, while the column spacing, column diameter, and friction angle of the embankment fill have a large effect on the load efficiency. The 2D numerical analysis of a physical model by Boussetta et al. [12] showed that the load efficiency increases with the increase of the cover ratio. This result was confirmed by Lee et al. [13].

Different analytical methods are used to design the rigid inclusion-supported embankment. The analytical method proposed by Abusharae et al. [14] showed that the load efficiency increases as the soft soil layer thickness decreases. Zhuang et al. [15] developed a new analytical method of design and found that the load efficiency increases if the geosynthetic stiffness increases and the soft soil stiffness decreases. Pham [16] proposed a new design method, the parametrical analysis based on this method was conducted, the results indicated that the load efficiency increases when the cover ratio, internal friction angle of embankment soils and embankment height increase.

The paper discusses the effect of geosynthetic and the optimum positions of these reinforcement layers on the load efficiency, moreover, this paper investigates the differences

between the changeable cover ratio by enlarging the column cap or the column cross-section area on the load efficiency and column behavior.

## II. Geometry of the Supported Embankment

A rigid inclusion-supported embankment located over different layers of soft soils was simulated by the finite element method (Plaxis 3D CONNECT Edition V20 program is adopted in the analysis). The soil profile is shown in *Fig. 1*. The levels of the soil layers are related to the NGF (French georeferenced level) [17].

Fig. 1. The soil profile

A working platform was applied before the construction stages. The columns were driven to be anchored to a gravel layer. The column spacing and diameter are respectively (1.6m, 0.274m). two layers of a geogrid were inserted in the load transfer platform with a thickness equal to 0.7m. the position of these two layers are 0.2m and 0.4m over the column heads [17].

The height of the embankment is 3.8m, the width of the embankment at the crest is 7m and at the base is 12m as shown in *Fig. 2*. The properties of the embankment fill, platform working soil, and column material are tabulated in *Table 1*.
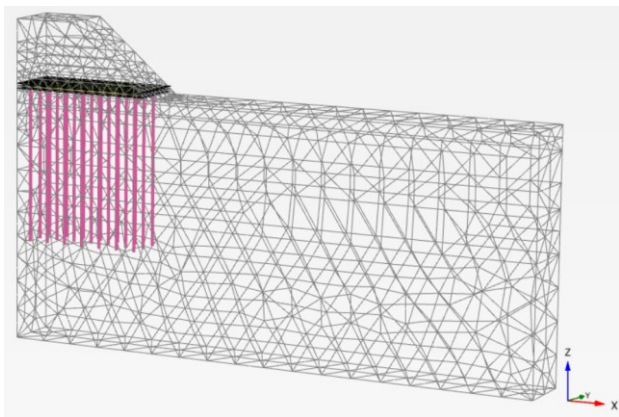
Fig. 2. Supported embankment by rigid inclusions and two layers of geogrid.

Soft Soil Creep (SSC) model was used to simulate the behavior of the soft soils. Hardening Soil (HS) model was used to simulate the behavior of the embankment fill, the working platform soil, and the gravel. The columns are modeled as embedded beam elements and the stiffness of the geogrid equal to 13000 kN/m.

TABLE I. PROPERTIS OF SOIL AND COLUMN MATERIAL.

| Embankment fill | | |
|---|---|---|
| $\gamma$ = 21 kN/m³ | $\varphi$=35° | $\Psi$=5° |
| c=5 kPa | E= 16000 kPa | k=0.864 m/day |
| Working platform soil | | |
| $\gamma$ = 21 kN/m³ | $\varphi$=35° | $\Psi$=5° |
| c=5 kPa | E= 12860 kPa | k=0.864 m/day |
| Column | | |
| $\gamma$= 24 kN/m³ | E=20 GPa | $\nu$=0.2 | L=12.7 m |

## III. Results and Discussion

### A. Effect of rigid inclusion on the embankment settlement

Due to the significant settlement problem of the embankments over soft soil layers, different technologies are used to reduce these settlements and increase the stability of the soil. *Fig. 3* shows the difference between the unsupported embankments, supported embankments by two layers of the geogrid located in the working platform, and supported embankments with rigid inclusions and two layers of geogrid. Rigid inclusion contributes to reduce the settlements at the embankment surface to reasonable values, especially for the high embankments.
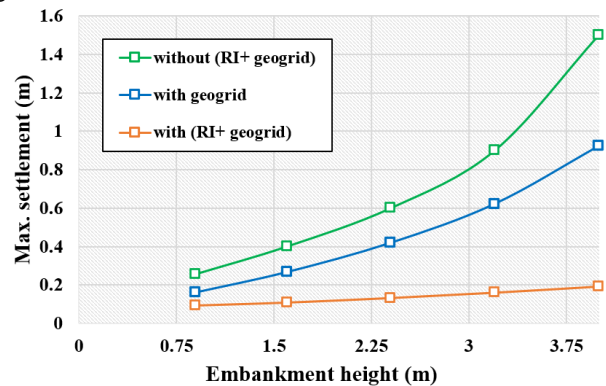
Fig. 3. Maximum settlements at the embankment surface for different heights

### B. Effect of geogrid layers on the load efficiency

The soil arching phenomenon is noticeable in the supported embankments whether the geogrid reinforcement is used or not, while the tensioned membrane phenomenon is relating to the presence of the geogrid layers. The geogrid stretch and subsoil settlement occur simultaneously, these phenomena contribute to mobilize the tensile forces in the geogrid layers and as a result, increase the load efficiency. *Fig. 4* shows the effect of using the geogrid layers on the load efficiency during the construction stages and consolidation period. It is evident that the load efficiency increases by about (60%) when one layer of geogrid is used and by about (63%) when two layers are used. Generally, using one layer is considered an effective and economical solution.

The position of the geogrid layer plays an important role in transferring the load to the rigid columns. Different positions of the geogrid layer were investigated to find out the effects on the load efficiency, the hypothetical positions of this layer are
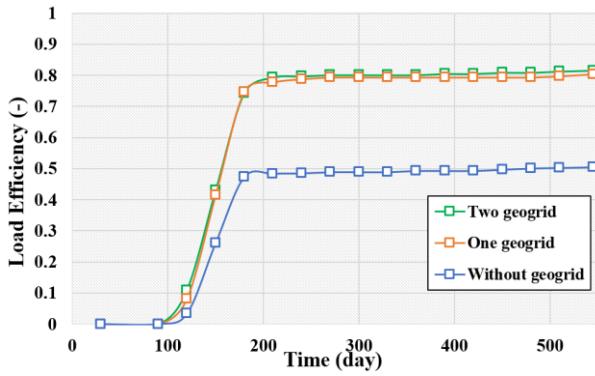
Fig. 4. Effect of geogrid on the load eeficiency.



Fig. 6. Effect of the the second geogrid layer position on the load efficiency.

(0, 0.2, 0.5) m above the column head. The load efficiency reaches its maximum (E=0.88) when the single geogrid layer located directly over the column head as shown in *Fig. 5*. The attribution of that, the lower the layer position, the higher the load applied on the geogrid layer. this load moves later to the column head.
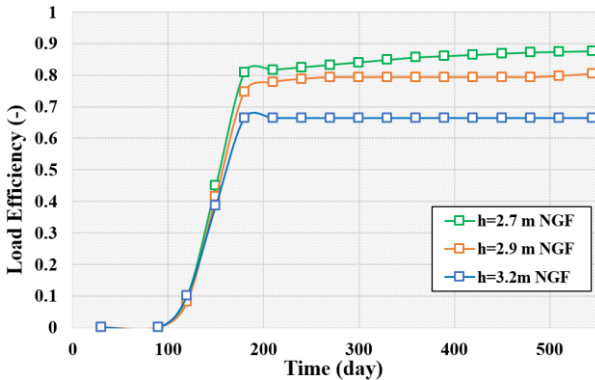


Fig. 5. Effect of the the first geogrid layer position on the load efficiency.

Next step after finding the optimum position of the first layer of geogrid is to find the position of the second layer (if any). The position of first layer is located directly over the column heads. Different positions of the second layer were investigated to find the effect on the load efficiency, the hypothetical positions of the second layer are (0, 0.2, 0.3, 1.02, 1.52) m over the column head. Insertion of this layer leads to decrease or increase the load efficiency between (2-5%). *Fig. 6* indicates that the effect of this layer cab be negligible. The results of the numerical analysis comply with those obtained from the experimental tests of van Eekelen et al. [3]. The researchers found that the behavior of the load distribution is approximately the same when one or two layers are placed in the embankment body.

*C. Effect of cover ratio on the load efficiency*

Based on the reference case, numerous numerical analyses were performed to determine the effects of cover ratio on the load efficiency and the behavior of axial forces along the column. The cover ratio ranges from (3%) to (27%) in the analysis, these percentages correspond to a range of column diameter (0.25-0.8) m suggested by ASIRI [1].
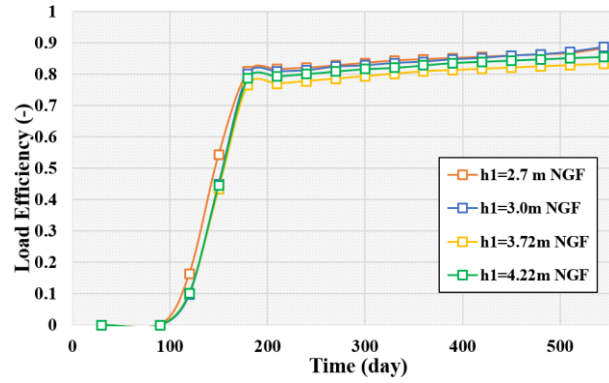
Two cases are discussed in this paper: Case A - increased cover ratio by enlarging the column cap; Case B – increased cover ratio by enlarging the cross- sectional area of the column.

*Fig. 7* shows that the load efficiency increases as the cover ratio increases according to case (A), and decreases as the cover ratio increases according to case (B).

In case (B), the skin friction zone increases and the shear forces resulting from the negative skin friction increases while the applied load on the column head decreases. *Fig. 8* shows the distribution of the axial forces for both cases (A and B) for two values of cover ratio ($\alpha$= 9%, $\alpha$= 15%).
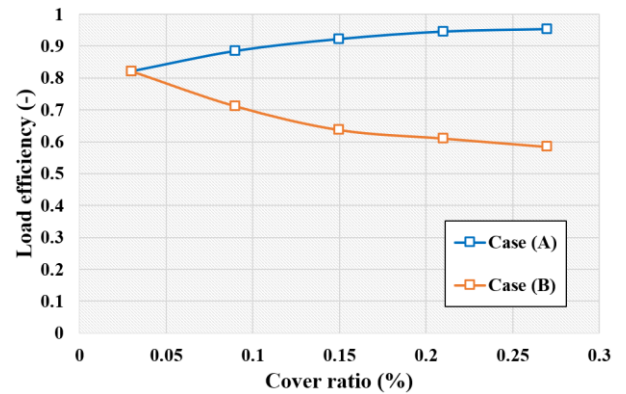


Fig. 7. Effect of cover ratio on the load efficiency in two cases (A),(B).

For the embankments supported by rigid inclusions and two layers of geogrid, the curves were plotted with different load efficiencies to be used for the preliminary design purpose as shown in Fig. 9. These curves comply relatively with several history cases [18] taking into consideration the effect of the possible differences (thickness of the load transfer platform, characteristics of the embankment fill, stiffness of the geogrid, stiffness and thickness of the soft soil layers, etc).

The cover ratios, for embankments with heights (H/(s-a) <1), is high in comparison with those, for embankments with heights (H/(s-a) >1) as shown in Fig. 9. On this basis, these curves provide a new criterion for classifying low and high embankments, where H is the embankment height, s is the column spacing, and a is the column diameter.
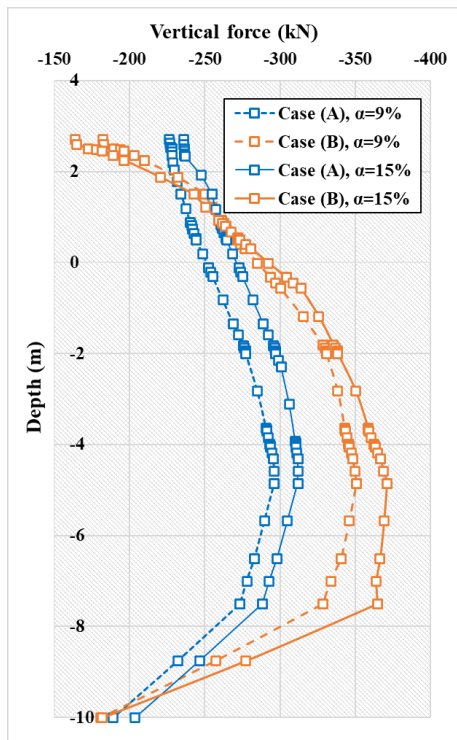
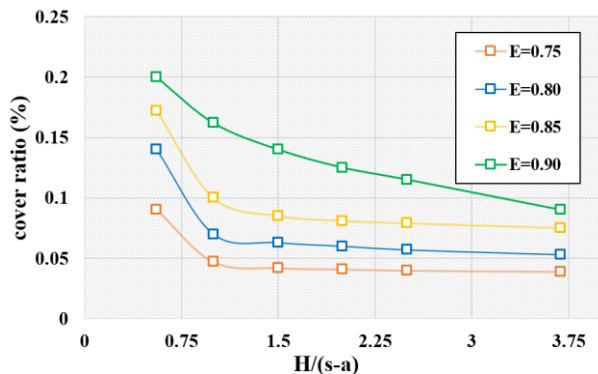Fig. 8.   Distribution of axial forces in the column in two cases (A),(B).



Fig. 9.   Correlation between cover ratio of column cap and embankment height.

## IV.  CONCLOUSIONS

Based on the numerical model of the embankment supported by rigid inclusions and two layers of geogrids, a parametric study was carried out, which yielded the following results:

1.  The rigid inclusions help to reduce the settlements of the embankment to a reasonable value.

2.  Inserting the geogrid layers in the load transfer platform helps to increase the load effeciency due to the transfer a part of the load by these layers to the column head. The results show that the load efficiency increases by (60%) if one layer is used and (63%) if two layers are used.

Therefore, the use of a single geogrid layer is considered an effective and economical.

3.  The position of the single geogrid layer plays an important role in transferring the load to the rigid columns. The maximum load efficiency occurs when the geogrid layer is located directly over the column head.

4.  The effect of using the second geogrid layer can be neglegable. The load efficiency increases or decreases between (2-5%), the optimal position can be directly above the first geogrid layer.

5.  The increase of the cover ratio by enlarging the column cap leads to increase the load efficiency while the increase of the cover ratio by enlarging the column cross-sectional area leads to decrease the load efficiency.

6.  In the case of enlarging the column cross-sectional area, the skin friction zone increases, and the shear forces resulting from the negative skin friction in the upper part of the colum increases while the applied load on the column head decreases.

7.  The curves in *Fig. 8* with different load efficiencies can be used for preliminary design.

8.  The cover ratio decreases as the embankment height increases, the limitation (H/(s-a) =1) can be accepted as a criterion to distinguish between low and high embankments.

[1]  IREX. Recommendations for the design, "construction and control of rigid inclusion ground improvements," Project National ASIRI. Presses des Ponts, Paris, p. 316, 2012.

[2]  R. Alsirawan, "Review of Geosynthetic-Reinforced Pile-Supported (GRPS) embankments - parametric study and design methods," Acta Technica Jaurinensis, Győr, vol. 14, December 2020, pp. 36-59.

[3]  S.J.M van Eekelen, A.Bezuijen, H.J.Lodder, A.F.van Tol, "Model experiments on piled embankments. Part I," Geosynthetics International, vol. 32, 2012, pp. 69-81.

[4]  R. Girout, M. Blanc, L. Thorel, D. Dias, "Geosynthetic reinforcement of pile-supported embankments," Geosynthetics International, vol. 28, February 2018, pp. 37-49.

[5]  O. Jenck, D. Dias, R. Kastner, "Two-Dimensional Physical and Numerical Modelingof a Pile-Supported Earth Platform over Soft Soil," Journal of Geotechnical and Geoenvironmental Engineering, vol. 133, March 2007, pp. 295-305.

[6]  M. Blanc, G. Rault, L. Thorel, M. Almeida, "Centrifuge investigation of load transfer mechanisms in a granularmattress above a rigid inclusions network," Geotextiles and Geomembranes, vol. 36, January 2013, pp. 92-105.

[7]  C. Xu, S. Song, J. Han, "Scaled model tests on influence factors of full geosynthetic-reinforced pile-supported embankments," Geosynthetics International, vol. 23, Novemebr 2015, pp. 1-14.

[8]  U.S.Okyay, D.Dias, "Use of lime and cement treated soils as pile supported load transfer platform," Engineering Geology, vol. 114, June 2010, pp. 34-44.

[9] J.Han, A.Gabr, "Numerical Analysis of Geosynthetic-Reinforced and Pile-Supported Earth Platforms over Soft Soil," Journal of geotechnical and geoenviromental engineering, vol. 128, January 2002, pp. 44-53.

[10] B. Le Hello, P. Villard, "Embankments reinforced by piles and geosynthetics—Numerical and experimentalstudies dealing with the transfer of load on the soil embankment," Engineering Geology, vol. 106, March 2009, pp. 78–91.

[11] M.Wijerathna, D. S.Liyanapathirana, "Loadtransfer mechanism ingeosynthetic reinforced column-supported embankments," Engineering Geology, vol. 27, June, 2020, pp. 236-248.

[12] S. Boussetta, M. Bouassida, M. Zouabi, "Assessment of observed behavior of soil reinforced by rigid inclusions," Innovative Infrastructure Solutions, vol. 1, August 2016, pp. 1-12.

[13] S. C. Lee, C. F. Leung, Y. K.Chow, "Performance of Oil Tank Foundation," GSP 132 Advances in Deep Foundations, Texas, United States, January 2005.

[14] S. W. Abusharar, J. J. Zheng, B.G.Chen, J. H. Yin, "A simplified method for analysis of a piled embankment reinforced with geosynthetics," Geotextiles and Geomembranes Journal, vol. 27, August 2008, pp. 39–52.

[15] Y. Zhuanga, K. Y. Wang, H. Liu, "A simplified model to analyze the reinforced piled embankments," Geotextiles and Geomembranes, vol. 42, 2014, pp. 154-165.

[16] T. A. Pham, "Analysis of geosynthetic-reinforced pile-supported embankment withsoil-structure interaction models," Computers and Geotechnics, vol. 121, May 2020.

[17] R. Alsirawan, E. Koch, "The finite element modeling of rigid inclusion-supported embankment," Pollack Periodica, In press.

[18] J. Han, "Design and construction of embankments on geosynthetic reinforced platforms supported by piles," Proceedings of 1999 ASCE/PaDOT Geotechnical Seminar, Central Pennsylvania Section, ASCE and Pennsylvania Department of Transportation, Hershey, pp. 66-84.